EAI Endorsed Transactions
on Industrial Networks and Intelligent Systems Research Article EAI.EU

Joint Adaptive Modulation and Power Control Scheme for Energy Efficient FSO-based Non-Terrestrial Networks

Thang V. Nguyen[1], Hien T. T. Pham[2,*], and Ngoc T. Dang[3]

[1,2,3]Wireless Systems and Applications Lab., Posts and Telecommunications Institute of Technology, Hanoi 100000, Vietnam

Abstract

Free-space optics (FSO)-based non-terrestrial networks (NTN) have garnered significant attention as a potential technology for forthcoming 6G wireless communications due to their exceptional data rate and extensive global coverage capability. Nevertheless, atmospheric attenuation, cloud attenuation, geometric loss, and atmospheric turbulence present numerous difficulties in developing these networks. To cope with these difficulties, we propose to apply a joint adaptive modulation and power control (JAMPC) scheme to FSO-based NTN. Our proposed JAMPC algorithm aims to enhance energy efficiency while guaranteeing the targeted outage probability, bit-error rate, and the required data rate. We develop mathematical models and derive closed-form expressions to implement the proposed algorithm and solve the optimization problem. The numerical results confirm that the JAMPC scheme helps NTN provide better energy efficiency and the ability to adapt to various channel conditions.

Keywords: Satellite communications, Free-space optics communications, Cloud attenuation, Atmospheric turbulence, Adaptive modulation, Power control.

Received on 20 09 2024; accepted on 1 12 2024; published on 3 12 2024

doi:10.4108/eetinis.v12i1.7317

1. Introduction

The provision of high-quality education, remote health interventions, skill training, and access to distance work possibilities can enhance individuals' quality of life through the utilization of broadband Internet connections. These benefits contribute to achieving prosperity and realizing the sustainable development goals initiative initiated by the United Nations. Although there is widespread worldwide digital connectivity, it is a verifiable reality that only 67% of the global population had access to the Internet in 2023, according to the [1]. The lack of adequate terrestrial infrastructure significantly hinders the establishment of reliable internet connectivity in remote settlements, thereby exacerbating the digital divide.

Continual endeavors are underway to attain widespread, efficient, and economical Internet connectivity via advancing non-terrestrial networks (NTN), which consist of satellites, high-altitude platforms (HAP) (e.g., balloons, airships, aircraft, etc.), low-altitude platforms (e.g., drones, helicopters, small-UAVs, and so on). According to [2], plans are being made to connect faraway places with low-earth orbit (LEO) satellite constellations to get around the problems of latency and adaptability that come with geosynchronous Earth orbit (GEO) communication systems. To ensure uninterrupted services, LEO satellites must deploy the complete constellation. As of November 2023, SpaceX has successfully deployed a total of 5,500 satellites. Similarly, as of May 2023, OneWeb has successfully launched 634 satellites. Furthermore, Telesat has outlined its intention to offer global Internet access by 2025, utilizing a fleet of 298 satellites. This is mostly attributed to the scarcity of the radio frequency (RF) spectrum on which these systems depend.

*Corresponding author. Email: hienptt@ptit.edu.vn

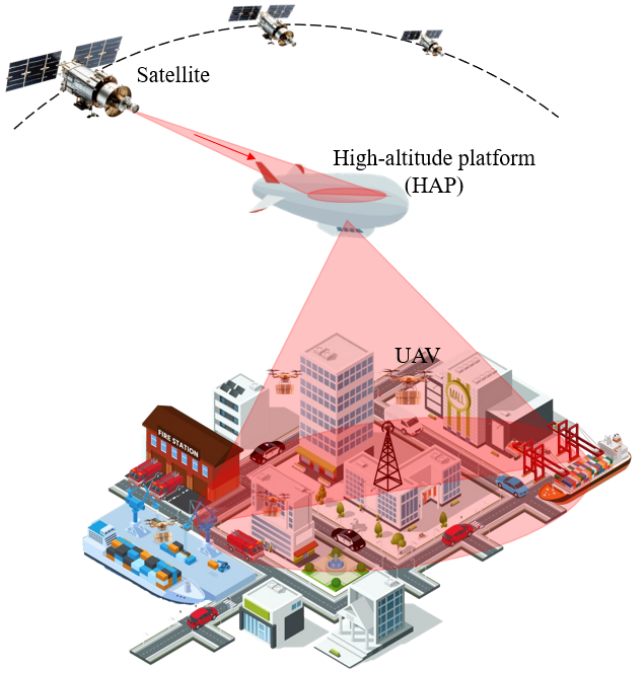

Figure 1. FSO-based non-terrestrial networks.

On the other hand, free-space optics (FSO) are being investigated as an inexpensive substitute for RF transmissions to overcome this issue [3]. The unlicensed spectrum, which has a wide operational capacity and is therefore significantly less expensive than RF, is advantageous for FSO. FSO is a good option for establishing a fast, secure connection to a base station with a high traffic demand. Therefore, combining NTN with FSO transmissions is a desirable option for broadband Internet access.

However, clouds, haze, fog, and atmospheric turbulence, significantly deteriorate the FSO link's effectiveness. Over the past decade, a great deal of attention has been paid to carrying out comprehensive research to find effective methods for addressing the aforementioned pressing concerns. One approach that might be effective is adaptive transmission, which adaptively changes the transmission rate, modulation scheme, and coding rate based on the channel conditions. Another efficient technique to raise the quality of an FSO link is to use relay-assisted transmission, which places intermediary nodes between the source and the destination [4].

It should be noted that most of the recent developments in the field of FSO-based NTN have focused on multi-rate adaptation systems. These systems operate under varying constellation sizes and must adhere to specific resource limitations and quality of service (QoS) criteria [5, 6]. The study conducted in [5] focused on designing and analyzing adaptive rate control for hybrid FSO/RF satellite communications systems using HAP-aided relaying. In [6], the authors presented a cross-layer design for a hybrid automatic repeat request-based sliding window mechanism and rate adaptation from a satellite in LEO to a station on Earth. This design was implemented while considering the constraint of bit-error rate (BER).

While the adaptive rate has the potential to greatly improve the rate of transmitted data and overall throughput performance, it is important to note that the transmission should also be controlled adaptively with the channel conditions for more efficient modulation control. The join utilization of adaptive rate and power control can effectively exploit advantageous channel conditions; hence, it significantly improves the system performance while maintaining the BER [7]. In comparison to non-adaptation and single-parameter adaptation techniques, these approaches have demonstrated their robustness. Several studies have been done on the optimization problem of maximizing or minimizing a certain performance metric, like spectral efficiency [7–9], the number of bits carried per chip time, or average power consumption [10]. However, these studies have mostly been done on RF and FSO-based terrestrial systems.

In this study, we propose to design an adaptive technique for an FSO-based non-terrestrial network that provides data transmission from a satellite to a UAV with the support of HAP-based relaying (see Figure 1). The main target of deploying FSO-based NTN is to support Gigabit connections to satisfy the requirement of the future 6G network; thus, the priority of the NTN is to select FSO-based transmission. In the case, the FSO is severely affected by environment-induced issues such as atmospheric turbulence, clouds, etc.; the RF is chosen as a backup link. Unlike previous studies that emphasize the utilization of only bit rate or modulation level adaptation strategies for achieving maximum transmission bit rate, our study proposes the adoption of joint adaptive modulation and power control (JAMPC) schemes to enhance the energy efficiency of NTN. The paper's primary contributions can be briefly stated as follows:

- We develop a joint adaptive modulation and power control algorithm for NTN, which first sets the modulation size and then determines the transmission power adaptively to the channel state while guaranteeing the required data rate and the BER.

- Based on the developed JAMPC algorithm, we build the mathematical model for implementing each algorithm step, where several search tools are applied to find the optimum thresholds.

- Finally, the closed-form expressions for average transmission power and energy efficiency are derived considering atmospheric attenuation, cloud effects, geometric loss, and turbulence-induced fading.

The subsequent sections of this work are structured in the following manner. Section 2 provides a comprehensive depiction of the channel models. In Section 3, we explain about NTN and our proposed JAMPC algorithm. Performance analysis of NTN using JAMPC algorithm is presented in Section 4. Section 5 provides numerical results and detailed explanations. Finally, this work is concluded in Section 6.

2. Channel Modeling

In this study, we consider a non-terrestrial network that provides data transmission from a satellite to a UAV supported by a HAP-based relaying node. The satellite is connected to the HAP through an FSO link, while the connection between the HAP and the UAV can be an FSO or RF link, depending on the channel conditions. In the case that the FSO channel from the HAP to the UAV is bad, the RF link will be used as an alternative. The main function of the HAP-based relaying node is to amplify and forward the signal.

2.1. FSO-based Satellite-to-HAP Link

Regarding the FSO-based satellite-to-HAP link, the impact of atmospheric turbulence is insignificant and may be disregarded since the laser beam travels over a path unaffected by the atmosphere (at an altitude of over 20 km, as opposed to ground level). For the sake of this work, we assume that HAP remains stationary at its designated location, and a precise fine-tracking system [11] is used with flawless alignment. Thus, it is presumed that the beam spreading loss significantly hinders the performance of this connection. In addition, the largest change in frequency between a LEO satellite and a stable HAP is typically a few gigahertz (GHz). This is within the capabilities of the present receiver design for LEO satellite-based FSO systems. These receivers can handle frequency shifts of over 10 GHz, as stated in the reference [12]. Consequently, the Doppler effect can be excluded from the performance analysis.

The collected power percentage at the circular detector of the HAP with an aperture radius D_{HAP} can be estimated based on the Gaussian beam profile as

$$h_{\mathrm{SH}} \approx A_0 \exp\left(-\frac{2\rho^2}{w_{L,\mathrm{e(eq)}}^2}\right), \tag{1}$$

where ρ is the radial distance from the beam center, $A_0 = [\mathrm{erf}(v)]^2$ represents the proportion of the total power collected at the point where $\rho = 0$, and $w_{L,\mathrm{e(eq)}}^2 = w_L^2 \frac{\sqrt{\pi}\mathrm{erf}(v)}{2v\exp(-v^2)}$ is the equivalent beam-waist, where $v = \frac{D_{\mathrm{HAP}}\sqrt{\pi}}{w_L\sqrt{2}}$ is defined as the ratio of the beam width and aperture radius. In addition, $w_L = w_0\sqrt{1+\epsilon\left(\frac{\lambda L_{\mathrm{SH}}}{\pi w_0^2}\right)^2}$ is the beam-waist at the HAP-situated plane L_{SH}, which is determined by $L_{\mathrm{SH}} = (H_{\mathrm{SAT}} - H_{\mathrm{HAP}})/\cos(\xi_{\mathrm{SAT}})$, where H_{SAT} and H_{HAP} are the satellite's altitude and HAP's altitude compared to the Earth's surface, respectively. Also, ξ_{SAT} is the zenith angle of the satellite, $w_0 = (2\lambda)/(\pi\theta_{\mathrm{SAT}})$ is the beam-waist at $L_{\mathrm{SH}} = 0$ with θ_{SAT} is the divergence angle of the satellite, $\epsilon = \left(1 + 2\frac{w_0^2}{\rho_0^2 L_{\mathrm{SH}}}\right)$, and $\rho(L_{\mathrm{SH}}) = (0.55C_n^2 k_w^2 L_{\mathrm{SH}})^{-3/5}$ is the coherence length [13].

2.2. FSO/RF-based HAP-to-UAV Link

In this section, we present channel modeling for the HAP-to-UAV link using hybrid FSO/RF transmission using FSO. First, the channel coefficient of the FSO link, h_f, is modeled considering atmospheric attenuation, cloud effects, atmospheric turbulence-induced fading, and optical beam spreading loss. Next, the RF channel coefficient, h_r, is derived based on the free space path loss and small-scale fading.

1) FSO channel model

Atmospheric attenuation: The optical signal attenuates while propagating from the HAP to the UAV through the air segment because the composition of gas molecules and aerosol particles in the air absorbs the laser beam energy (i.e., absorption) and changes the direction of the light (i.e., scattering). The Beer-Lambert law is utilized to estimate the path loss h_f^l as follows [14]

$$h_f^l = \exp\left[-(\sigma_{at} + \sigma_{st})L_{\mathrm{HU}}\right], \tag{2}$$

where σ_{at} and σ_{st} are denoted as absorption attenuation and scattering attenuation coefficients, respectively. $L_{\mathrm{HU}} = (H_{\mathrm{HAP}} - H_{\mathrm{UAV}})/\cos(\xi_{\mathrm{HU}})$ is the propagation length of the FSO link in which ξ_{HU} is the zenith angle of the HAP-to-UAV link. Table 1 shows the values of σ_{at} and σ_{sc} at the optical wavelength of $\lambda = 1550$ nm [15].

Cloud attennuation: As reported in [16], large cloud cover increases the likelihood that the optical beam from the satellite to the ground will be obstructed, particularly in regions that experience severe weather like storms, floods, heavy rain, etc. Thus, this study looks into the effects of clouds. Due to high attenuation, clouds have a significant critical effect on the FSO link, as was recently observed in [17]. System availability and performance may suffer significantly when cloud

Table 1. Attenuation coefficient for different conditions.

Atmospheric coeff.			
	Absorption σ_{at} (km^{-1})	Heavy fog	28.75
		Light fog	4.6
		Haze	0.966
		Clear air	0.0989
	Scattering σ_{st} (km^{-1})	Extreme volcanic	10^{-1}
		High volcanic	2×10^{-2}
		Moderate volcanic	8×10^{-4}
		Background volcanic	10^{-4}

coverage is present because of high CLWC. The Beer-Lambert law can be used to express cloud attenuation.

$$h_f^{\mathrm{c}} = \exp\left(-\alpha_c d_{\mathrm{c}}\right), \tag{3}$$

where α_c is the attenuation coefficient and can be expressed as

$$\alpha_c = \frac{3.91}{V\,[\mathrm{km}]}\left(\frac{\lambda\,[\mathrm{nm}]}{550}\right)^{-q}, \tag{4}$$

where q is the coefficient of Kim's model [17]. The visibility can be determined based on cloud droplet number concentration N_{c} and cloud liquid water content M_{c} as followed

$$V = \frac{1.002}{\left(N_{\mathrm{c}} \times M_{\mathrm{c}}\right)^{0.6473}}. \tag{5}$$

The typical values of N_{c} and M_{c} for multiple types of clouds are presented in [18].

Beam spreading loss: similar to (1), the fraction of the power collected by UAV with the aperture radius of D_{UAV} can be approximated as

$$h_f^{\mathrm{s}} \approx A_0 \exp\left(-2\left(\frac{r_{UAV}}{\omega_{L,\mathrm{e(eq)}}}\right)^2\right), \tag{6}$$

where r_{UAV} is the radial displacement between centers of HAP beam footprint and UAV's detector, $\omega_{L,\mathrm{e(eq)}}$ is the equivalent beam waist, and $A_0 = [\mathrm{erf}(v)]^2$ with $v = \sqrt{\pi} D_{\mathrm{UAV}}/(\sqrt{2}\omega_{L,\mathrm{e}})$. Additionally, $\omega_{L,\mathrm{e}} \approx \theta_{\mathrm{HU}} L_{\mathrm{HU}}$, where θ_{HU} is the divergence angle for the HAP-UAV beam, and L_{HU} is the propagation distance from HAP to UAV.

Atmospheric turbulence-induced fading: The inhomogeneity of temperature and pressure in the atmosphere causes variations in the refractive index of the air, which in turn causes atmospheric turbulence. It results in variations in the received optical intensity, which considerably lowers the free-space channel's efficiency. Let's look at an electromagnetic wave that travels through a turbulent atmosphere with a random refractive index. Given the fading channel coefficient, a well-known Gamma-Gamma distribution is applied to represent its probability density function (PDF) and can be shown as

$$f_{h_f^t}(h_f^t) = \frac{2(\alpha\beta)^{\frac{\alpha+\beta}{2}}}{\Gamma(\alpha)\Gamma(\beta)} (h_f^t)^{\frac{\alpha+\beta}{2}} K_{\alpha-\beta}\left(2\sqrt{\alpha\beta h_f^t}\right), \tag{7}$$

where $K_{\alpha-\beta}(\cdot)$ is the $(\alpha-\beta)$-th order modified Bessel function of the second kind [19]. In addition, the parameters α and β correspond to the number of large-scale and small-scale air pockets of the scattering environment and can be directly linked to physical parameters as

$$\alpha = \left[\exp\left(\frac{0.49\sigma_R^2}{\left(1 + 1.11\sigma_R^{12/5}\right)^{7/6}}\right) - 1\right]^{-1}, \tag{8}$$

$$\beta = \left[\exp\left(\frac{0.51\sigma_R^2}{\left(1 + 0.69\sigma_R^{12/5}\right)^{5/6}}\right) - 1\right]^{-1}, \tag{9}$$

where σ_R^2 is the Rytov variance, which usually measures the turbulence strength. Notably, σ_R^2 is used to define weak, moderate, and strong turbulence corresponding to $\sigma_R^2 < 1$, $\sigma_R^2 \approx 1$, and $\sigma_R^2 > 1$, respectively. In the case of plane wave propagation, the Rytov variance is given as [20]

$$\sigma_R^2 = 2.25 k^{7/6} \sec^{11/6}(\xi) \int_{H_{\mathrm{UAV}}}^{H_{\mathrm{HAP}}} C_n^2(h) \left(h - H_{\mathrm{UAV}}\right)^{5/6} dh, \tag{10}$$

where $C_n^2(h)$ is the variation of the refractive index structure parameter described by the Hufnagel-Valley model [16] and can be expressed as

$$C_n^2(h) = 0.00594\left(\frac{v_{\mathrm{wind}}}{27}\right)^2 \left(10^{-5}h\right)^{10} \exp\left(-\frac{h}{1000}\right) + 2.7 \times 10^{-16} \exp\left(-\frac{h}{1500}\right) + C_n^2(0) \exp\left(-\frac{h}{100}\right), \tag{11}$$

where $C_n^2(0)$ is the ground level turbulence, and v_{wind} (m/s) is the root mean squared wind speed.

2) RF Channel Model In the considered FSO-based NTN, we aim to achieve the gigabit transmission to satisfy the requirement of the future 6G network; thus the optical link is used as the first priority. However, the FSO link is vulnerable due the effect of the troposphere layer as mentioned in the previous section; hence, the RF link is proposed to operate like a backup link, which is activated whenever FSO link cannot meet the quality of service demand. The system can switch to RF-based transmission mode when the FSO-based transmission encounters difficulties. Hence, in analyzing the RF channel, we take into account the

primary obstacles, such as propagation loss, attenuation induced by clouds, and fading phenomena. The channel coefficient of the RF connection can be mathematically represented as $h_{\mathrm{HU}}^{r} = g_r h_r$. Here, h_r represents the channel fading coefficient, and g_r represents the path-loss of the RF link, as stated in the reference[21].

$$g_r(\mathrm{dB}) = G_{\mathrm{T}} + G_{\mathrm{R}} - \mathcal{L}_{\mathrm{F}} - \mathcal{L}_{\mathrm{A}} - \mathcal{L}_{\mathrm{c}}, \tag{12}$$

where G_{T} and G_{R} represent the antenna gains of the transmitter and receiver, measured in decibels (dB), respectively. The term $\mathcal{L}_{\mathrm{A}}$ (dB) refers to the loss of signal strength in the atmosphere due to gaseous factors. The equation $\mathcal{L}_{\mathrm{F}}(\mathrm{dB}) = 92.45 + 20\log f_c + 20\log L_{\mathrm{HU}}$ represents the free space loss for a radio frequency (RF) link between the HAP and the UAV. The frequency of the RF link is given by f_c, which is measured in gigahertz, and L_{HU} is the propagation distance from HAP to UAV.

Regarding the attenuation induced by clouds, according to ITU-P840 [22], the Rayleigh scattering model is appropriate for representing the decrease in signal strength up to 200 GHz. In this model, the attenuation caused by clouds on a RF link can be described as [22]

$$\mathcal{L}_{\mathrm{c}} = \frac{d_{\mathrm{c}}^{r}\alpha_r}{\cos(\xi_{\mathrm{HU}})}, \tag{13}$$

where d_{c}^{r} denoted as RF transmission link length affected by clouds, and $\alpha_r = K_{\mathrm{c}}M_{\mathrm{c}}$ is defined as the specific attenuation within clouds in which K_{c} represents the specific attenuation coefficient in $((\mathrm{dB/km})/(\mathrm{g/m^3}))$, M_{c} $(\mathrm{g/m^3})$ denoted as the CLWC as shown in [22].

As for the fading model, the Rician distribution is commonly used to characterize the small-scale fading in the vertical link from HAP to UAV, which is influenced by the line-of-sight (LOS). Hence, the PDF of the fading coefficient for the RF channel, represented by the symbol h_r, can be expressed as stated in the reference [23]

$$f_{h_r}(h_r) = \frac{2(K_R+1)h_r}{\Omega}\exp\left(-K_R - \frac{(K_R+1)h_r^2}{\Omega}\right) \times I_0\left(2\sqrt{\frac{K_R(K_R+1)h_r}{\Omega}}\right), \tag{14}$$

where Ω is the total power from both paths, i.e., the direct path and scattered paths [24]. K_R is the Rician factor with the typical value of 6 dB [25].

3. Non-Terrestrial Network with JAMPC

3.1. System Descriptions

Figure 2 illustrates an optical non-terrestrial network utilizing the JAMPC approach. In our considered

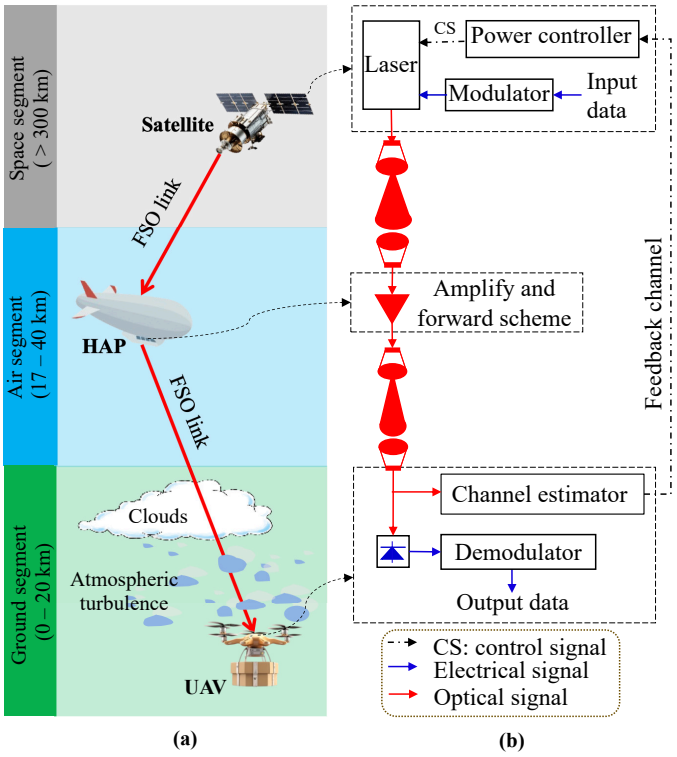

Figure 2. FSO-based NTN: (a) Network model and (b) Block diagram.

system, as depicted in Fig. 2(a), the satellite, situated at the space segment, is a source node. The HAP, located at the air segment, serves as a relay node that amplifies the strength of the optical signal received from the satellite and subsequently transmits it to the intended destination. UAVs play a role as a destination node, which is deployed to perform ground segment applications such as serving irregular events (concerts, sports, etc.), restoring telecommunications infrastructure in areas affected by natural disasters, providing logistics support services, and assisting intelligent vehicular networks.

In order to achieve system efficiency in both energy and transmission bit rate to satisfy application requirements in 6G networks, the JAMPC scheme is implemented. As illustrated in Fig. 2(b), the data is first modulated and sent by the satellite to HAP via the FSO link.

The received signal at HAP, which was transmitted from satellite through the FSO link, is given as

$$y_{\mathrm{S}} = h_{\mathrm{SH}}P_t s_{\mathrm{m}}(t) + n_{\mathrm{SH}}, \tag{15}$$

where P_{t} is the satellite's transmitted power, $s_{\mathrm{m}}(t) = r_{\mathrm{m}}\cos(2\pi f_c t + \theta_{\mathrm{m}})$ is the transmitted M-ary quadrature amplitude modulation (M-QAM) signal from satellite, in which f_c is the sub-carrier frequency, r_{m} and θ_{m}

are the signal amplitude and phase, respectively. n_{SH} is the additive white Gaussian noise (AWGN) with zero-mean and variance σ^2_{SH} and h_f represents the channel coefficient of the FSO-based satellite-to-HAP link. At the HAP, the output of optical, denoted as y_{H}, can be written as $y_{\mathrm{H}} = A_{\mathrm{H}} y_{\mathrm{S}}(t)$ in which A_{H} is the amplifier gain. The optical signal is eventually forwarded to the UAVs through the atmosphere channel. Hence, the received signal at UAVs is given as

$$\begin{aligned} y_{\mathrm{U}} &= h_f y_{\mathrm{H}}(t) + n_{\mathrm{HU}}, \\ &= A_{\mathrm{H}} h_{\mathrm{SH}} h_f P_t s_{\mathrm{m}}(t) + h_{\mathrm{SH}} n_{\mathrm{SH}} + n_{\mathrm{HU}}, \end{aligned} \tag{16}$$

where n_{HU} is the AWGN with zero-mean and variance σ^2_{HU}. Besides, $h = A_H h_{\mathrm{SH}} h_f$ is the end-to-end channel coefficient. We may set the amplifier gain at the HAP to compensate for the optical beam spreading loss at the first hop; hence, $h = h_f$ is used the input for the JAMPC algorithm.

In our study, the feedback channel transmitting channel state information (CSI) information, which is retrieved and included in the channel estimator to facilitate the implementation of the JAMPC algorithm, is expected to be reliable. On the other hand, the JAMPC algorithm can constantly monitor and adjust transmit power based on the real-time link quality. To cope with the rapid variations in atmospheric conditions, the JAMPC algorithm can be assisted by prediction algorithms, like Kalman filters, to estimate upcoming changes and preemptively adjust power levels. In addition, ground stations may handle complex optimization calculations. This allows the JAMPC algorithm to be responsive without relying heavily on onboard processing.

3.2. JAMPC Algorithm

The power control algorithm takes the values of the targeted outage probability ($\mathrm{Pr}_{out,tar}$), the required data rate (R_{req}), the targeted bit-error rate (BER_{tar}), and the current channel state (h) as the input. At the first step of JAMPC, the outage probability threshold, h^*_1, is calculated based on the given $\mathrm{Pr}_{out,tar}$. If the estimated channel state, h, is smaller than h^*_1, the system outage happens and the connection between HAP and UAV transitions to utilizing RF transmission. Otherwise, we partition the channel gain into smaller intervals created by a set of thresholds, $h^* = \{h^*_1, h^*_2, ..., h^*_{K+1}\}$. Each interval corresponds to a specific modulation size, M_i, determined by R_{req}. The algorithm selects the modulation order $M = \{M_1, M_2, ..., M_{K+1}\}$ by considering the current channel state, subject to the requirement that $h^*_i \le h \le h^*_{i+1}$, where i is an integer between 1 and $K+1$. In addition, $P_r = \{P_{r,1}, P_{r,2}, ..., P_{r,K+1}\}$, representing the received power thresholds, is determined by the QAM constellation vector M, which ensures a target bit error rate at the receiver. Furthermore, the feedback channel conveying CSI information is deemed credible, allowing for the employment of a robust error correction algorithm [26]. Furthermore, the temporal coherence periods of the FSO and RF links under consideration are rather long, i.e., in an order of ten milliseconds, when compared to the coherent time. This includes data transmission and feedback time, which are in the order of several milliseconds [25], owing to fading channels having a gradual and time-varying behavior. Because fading channels have a sluggish, time-varying nature, CSIs remain current when they reach the HAP and satellite; then, an error-free feedback channel is available for CSI [27]. Finally, the calculation of the transmission power is determined by $P_t(h) = \frac{P_{r,i}}{h'}$, where h' is the optimal value of h to achieve the minimal average transmission power. The details of PC algorithm are described in Algorithm 1.

Algorithm 1 Power control scheme for FSO links

Input: $\mathrm{Pr}_{out,\ tar}$, BER_{tar}, R_{req}, h
Step 1: Given P^{out}_{tar}, determine h^*_1
if $h > h^*_1$ **then**
Step 2: Given R_{req}, calculate h^*
Step 3:
3.1: Selecting modulation size M_i based on $h^*_i \le h < h^*_{i+1}$
3.2: Deciding transmission level $P_t(h) = \frac{P_{r,i}}{h'}$
Output: $P_t(h)$
else
Outage FSO mode (transitioning to RF mode)
end if

4. Performance Analysis

In the JAMPC algorithm, for a required data rate (R_{req}), we aim to minimize the average transmission power ($\bar{P}_t$) by changing the transmission power (P_t) while keeping the target outage probability ($P\,r_{out,tar}$) and the BER. The modulation size (M) and transmission power (P_t) in our adaptive systems will be dynamically adjusted based on the composite channel coefficient h, specifically designated as $M(h)$ and $P_t(h)$, respectively.

The JAMPC algorithm is mathematically modeled as

$$\min_{P_t(h),M(h)} \overline{P}_t = \int_0^{\infty} P_t(h) f_h(h) dh, \tag{17a}$$

$$s.t. R_{req} = \int_0^{\infty} R_s \log_2(M(h)) f_h(h) dh, \tag{17b}$$

$$\Pr_{out} \leq \Pr_{out,tar}, \tag{17c}$$

$$\mathrm{BER}(h) \leq \mathrm{BER}_{tar}, \tag{17d}$$

$$P_t(h) \leq P_{t,lim}, \tag{17e}$$

where $P_{t,lim}$ is the limited transmission power that the FSO transmitter can support.

The output of the JAMPC algorithm, i.e., the transmission power, can be calculated as follows

$$P_t(h) = \begin{cases} \frac{P_{r,i}}{h} & h_i^* \leq h < h_{i+1}^* \\ 0 & h < h_1^* \end{cases} \tag{18}$$

where h_1^* is the outage threshold, which can be determined by setting the outage probability to be equal to $Pr_{out,tar}$, i.e.,

$$\Pr_{out,tar} = \int_0^{h_1^*} f_h(h) dh = F_h(h_1^*), \tag{19}$$

where $F_h(.)$ is the cumulative distribution function (CDF). The optimization problem is now reduced to determine the optimal transmission thresholds h^* and can be written as

$$\min \overline{P}_t = \sum_{i=1}^{K} P_{r,i} \int_{h_i^*}^{h_{i+1}^*} \frac{f_h(h)}{h} dh \tag{20a}$$

$$s.t. R_{req} = \sum_{i=1}^{K} R_s \log_2(M_i) \int_{h_i^*}^{h_{i+1}^*} \frac{f_h(h)}{h} dh \tag{20b}$$

$$h_1^* \leq h_2^* \leq ... \leq h_{K+1}^*. \tag{20c}$$

By using the Lagrangian method shown in [28], an set of thresholds h^* can be derived as

$$h_i^*(\varsigma) = \frac{1}{\varsigma} \frac{P_{r,i} - P_{r,i-1}}{\log_2 K_i - \log_2 K_{i-1}}, \; i \in \{2, ..., K+1\}, \tag{21}$$

where ς is the Lagrange multiplier and can be obtained from

$$R_{req} = \sum_{i=1}^{K} R_s \log_2(M_i) \int_{h_i^*(\varsigma)}^{h_{i+1}^*(\varsigma)} f_h(h) dh$$

$$= \sum_{i=1}^{K} R_s \log_2(M_i) \left[F_h\left(h_{i+1}^*(\varsigma)\right) - F_h\left(h_i^*(\varsigma)\right) \right]. \tag{22}$$

It is worth noting that the Bisection search algorithm [29] is applied to find the h_i^* in Eq. (21).

This study aims to propose a method for enhancing the energy efficiency of NTN by utilizing JAMPC. Therefore, the performance metric, specifically energy efficiency ($\overline{\eta}_{EE}$), is examined to demonstrate the efficacy of our proposed JAMPC scheme. Energy efficiency is defined as the ratio of the average number of successfully received data bits (N_B) during a symbol's duration (T_s) to the average energy consumed in the same time interval. Mathematically, it may be expressed as

$$\overline{\eta}_{EE} = \frac{\overline{N}_b}{\overline{P}_t \times T_s}, \tag{23}$$

where N_b can be given as

$$\overline{N}_b = \sum_{1}^{N} R_k p_k (1 - \mathrm{BER}_k) \tag{24}$$

where R_k is the transmission rate at state k-th, BER_k is the bit error rate of selecting mode k-th over fading channel, which can be determined as

$$\mathrm{BER}_k^{FSO} = \frac{1}{p_k^{FSO}} \int_{h_f^i}^{h_f^{i+1}} \mathrm{BER}\left(h_f\right) f_{h_f}\left(h_f\right) dh_f \tag{25}$$

$$\mathrm{BER}_k^{RF} = \frac{1}{p_k^{RF}} \int_{h_r^i}^{h_r^{i+1}} \mathrm{BER}(h_r) f_{h_r}(h_r) dh_r \tag{26}$$

where p_k^{FSO} and p_k^{RF} are the transmission mode probabilities, which are defined as in [5]. In addition, the average transmission power, an important parameter in a power control scheme, can be determined as

$$\overline{P}_t = \sum_{i=1}^{K} \int_{h_i^*}^{h_{i+1}^*} \frac{P_{r,k}^{\mathrm{FSO}}}{h_f} f_{h_f}\left(h_f\right) dh_f$$

$$+ \Pr_{out,tar} \int_0^{h_r^*} \frac{P_r^{\mathrm{RF}}}{h_r} f_{h_r}(h_r) dh_r, \tag{27}$$

where K is the total number of FSO sub-transmission modes. $P_{r,k}^{\mathrm{FSO}}$ is the received power corresponding to the channel state k-th and can be determined by $P_{r,k}^{\mathrm{FSO}} = -\frac{2}{3}\sigma_n^2 (K-1) \ln(5\mathrm{BER}_{tar})$.

By applying [30, Eq. (14) and Eq. (26)], applying the Gauss-Hermit quadrature integration [31, (25.4.46)] together with some manipulations, the closed-form expression of average transmission power in Eq. (27) can be derived as in (28).

$$\bar{P}_t = \sum_{i=1}^{U} P_r^{FSO} \frac{(\alpha\beta)^{\frac{\alpha+\beta}{2}}}{\Gamma(\alpha)\Gamma(\beta)} \left[\left(h_{i+1}^*\right)^{\frac{\alpha+\beta}{2}} G_{1,3}^{2,1}\left(\alpha\beta h_{i+1}^* \middle| \begin{matrix} \frac{\alpha-\beta}{2} & \frac{\beta-\alpha}{2} \end{matrix} \begin{matrix} 1-\frac{\alpha+\beta}{2} \\ -\frac{\alpha+\beta}{2} \end{matrix}\right) - \left(h_i^*\right)^{\frac{\alpha+\beta}{2}} G_{1,3}^{2,1}\left(\alpha\beta h_i^* \middle| \begin{matrix} \frac{\alpha-\beta}{2} & \frac{\beta-\alpha}{2} \end{matrix} \begin{matrix} 1-\frac{\alpha+\beta}{2} \\ -\frac{\alpha+\beta}{2} \end{matrix}\right) \right]$$
$$+ \sum_{i=1}^{n} \Pr_{out,tar} P_r^{RF} \frac{2w_i(K+1)}{\Omega} \exp(-K) I_0\left(2\sqrt{\frac{K(K+1)}{\Omega}\sqrt{\frac{\Omega}{(K+1)}x_i}}\right). \quad (28)$$

Table 2. System Parameters

Name	Symbol	Value
LEO Satellite		
LEO satellite altitude	H_{SAT}	600 km
Divergence angle	θ_{SAT}	15 μrad
Satellite's zenith angle	ξ_{SAT}	10°
High Altitude Platform (HAP)		
HAP altitude	H_{HAP}	20 km
HAP's aperture radius	D_{HAP}	10 cm
HAP's divergence angle	θ_{HU}	4 mrad
HAP's zenith angle	ξ_{HU}	20°
Unnamed Aerial Vehicle (UAV)		
UAV altitude	H_{UAV}	2.5 km
UAV aperture diameter	D_{UAV}	10 cm
UAV's zenith angle	ξ_{UAV}	60°
Other Parameters		
Optical wavelength	λ	1550 nm
FSO symbol rate	R_s^f	250 Msps
Targeted BER	BER_{tar}	10^{-5}
Targeted outage probability	$\text{P}_{out,target}$	10^{-2}
Request bit rate	R_{req}	600 Mbps
Symbol time interval	T_s	1 ms
Cloud concentrations	N_c	250 cm^{-3}
Vertical extent of cloud	d_c^f	2 km
Cloud liquid water content	L_c	2 mg/m^3
Noise spectral density	σ_n^2	10^{-14}

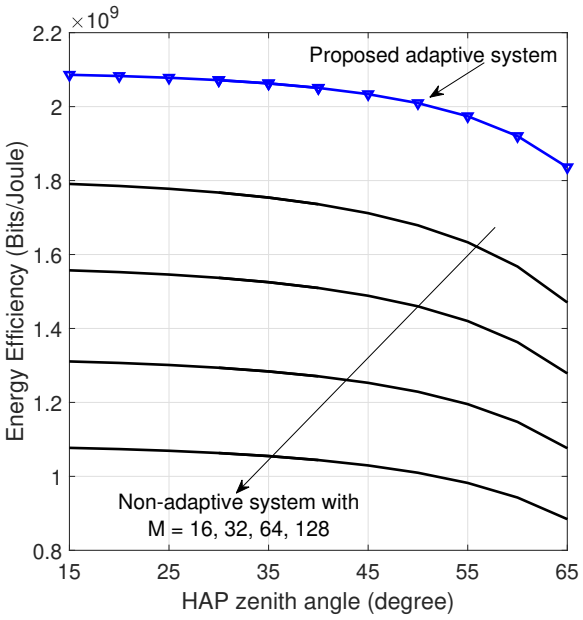

Figure 3. Energy efficiency of FSO-based NTN: the comparison between JAMPC and non-adaptive scheme.

5. Results and Discussions

In this section, we present numerical results for the energy efficiency in the considered FSO-based NTN with a power control technique. The modulation size is chosen from a set of $M \in \{4, 8, 16, 32, 64, 128\}$. Unless otherwise specified, system parameters utilized in this paper are listed in Table 2.

First, in Fig. 3, we investigate the energy efficiency of FSO-based NTN over the range of HAP's zenith angle for two cases, i.e., conventional NTN without adaptive modulation scheme and the proposed NTN with JAMPC. With the same symbol time, the energy required per bit increases as the bit rate increases. Consequently, the energy efficiency of non-adaptive NTNs deteriorates as the modulation size increases, that is, with higher bit rates. The reason for the low energy efficiency also comes from the use of fixed transmission power regardless of the channel conditions. In contrast, the variation of transmission parameters depending on the channel state thanks to JAMPC helps to reduce the BER (i.e., increase the average number of successfully received data bits) and save power. Therefore, the utilization of JAMPC can significantly boost the energy efficiency of the FSO-based NTN. For example, given the HAP's zenith angle of 45 degrees, JAMPC helps to gain about 300 Mbits/Joule in comparison with conventional FSO-based NTN with fixed modulation size $M = 16$ and non-adaptive transmission power.

Next, Figure 4 explores the energy efficiency of FSO-based NTNs in different application scenarios represented by different required bit rates, outage probabilities, and targeted bit error rates. For a specified targeted bit error rate, BER_{tar}, such as 10^{-6}, a lower necessary bit rate and/or a reduced outage

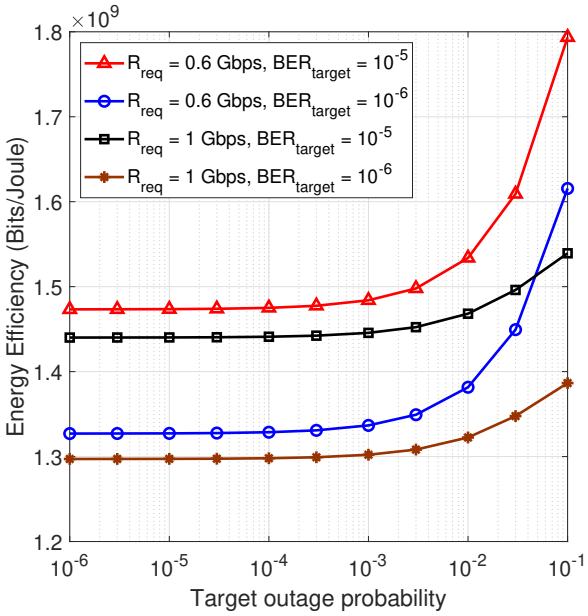

Figure 4. Influence of request rate, target outage probability, targeted BER on the energy efficiency.

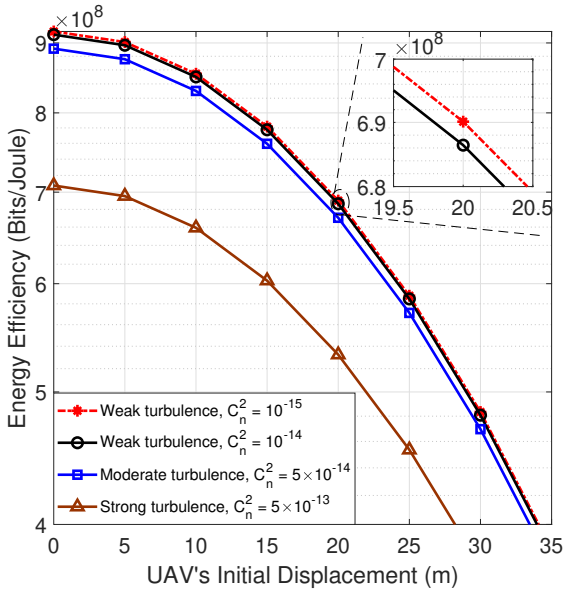

Figure 5. Energy efficiency versus UAV initial displacement for FSO-based NTN using JAMPC in three different turbulence strength conditions.

probability indicate greater energy efficiency. This is possible due to JAMPC's capability to adaptively reduce the transmission power in response to the lower demands of these parameters. With a targeted outage probability of 10^{-3}, an FSO-based NTN utilizing JAMPC can attain an energy efficiency of 1.3

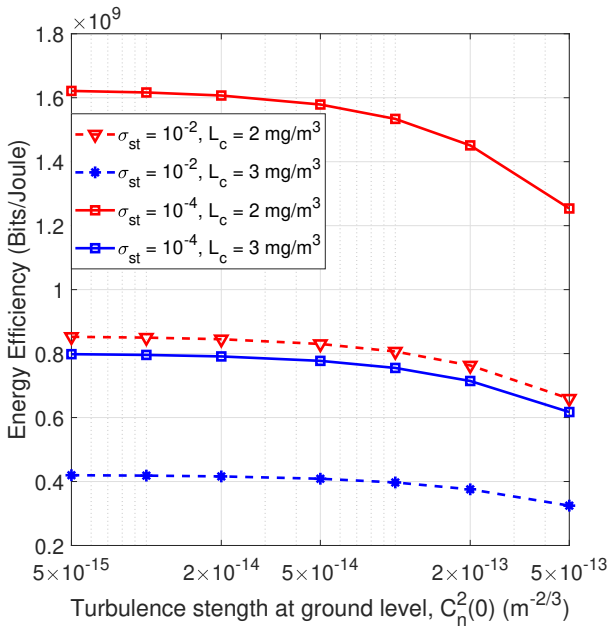

Figure 6. Exploring the effect of weather-related issues on energy efficiency over the range of turbulence strength at ground level.

Gbits/Joule at the necessary data rate of 1 Gbps and a BER of 10^{-6}.

Figure 5 depicts the correlation between the energy efficiency and the initial displacement of a UAV, represented as r_{UAV}. This denotes the distance from the center of the Gaussian beam to the UAV's initial position. This study examines the energy efficiency under three distinct environmental conditions of atmospheric turbulence including weak, moderate, and strong turbulence. It appears that the energy efficiency shows little difference between cases of weak and moderate turbulence. In contrast, strong turbulence leads to a substantial decrease in energy efficiency. Moreover, the initial displacement impacts energy efficiency as well. This is due to the fact that the received power diminishes significantly as the initial displacement increases. For example, with strong turbulence, energy efficiency decreases from 700 Mbits/Joule to 600 Mbits/Joule as the initial displacement grows from zero to 15 meters.

We investigate the impact of weather-related factors, such as cloud conditions and stratospheric layer conditions, on energy efficiency across a spectrum of turbulence strengths, $C_n(0)$, ranging from a weak regime (5×10^{-15}) to a strong regime (5×10^{-13}), as depicted in Fig. 6. In addition, we examine two stratospheric conditions: one with high volcanic activity where $\sigma_{st} = 10^{-2}$, and another with background volcanic activity where $\sigma_{st} = 10^{-4}$. Additionally, we

consider two cloud conditions, one with $L_c = 2$ mg/m^3 and the other with $L_c = 3$ mg/m^3. As evidenced by the preceding findings, this outcome reaffirms the notion that energy efficiency experiences a significant decline when exposed to strong atmospheric turbulence. With the high volcanic condition set at $\sigma_{st} = 10^{-2}$, 1 mg/m^3 increase in CLWC results in an energy efficiency decrease of approximately 0.4 Gbits/Joule. Conversely, under a similar cloud condition with $L_c = 2$ mg/m^3, the high volcanic condition significantly reduces energy efficiency, dropping it from 1.621 Gbits/Joule to 0.852 Gbits/Joule when comparing high and background volcanic conditions.

Finally, we examine the performance of NTN supported by a hybrid FSO/RF transmission that occurs during outage conditions of the FSO link from the HAP to the UAV. Various weather conditions are taken into account, such as a CLWC of 3 mg/m^3 and a CLWC of 2 mg/m^3, as depicted in Fig. 7. Under light cloud conditions, e.g., with a CLWC of $L_c = 2$mg/m^3, the NTN keeps FSO mode for the HAP-to-UAV link when the distance the between beam center and UAV position is smaller than 20 meters. In this case, the outage probability is 10^{-2}. When the distance between the beam center and the UAV position is larger than 20 meters and $L_c = 3$mg/m^3, the received power from a narrow FSO beam becomes so low that it results in an outage of the FSO mode. As a result, the NTN transitions to a hybrid FSO/RF transmission, and the overall outage probability is approximately 2×10^{-7}. This result confirms that a hybrid FSO/RF transmission is effective regarding the outage performance as proved in several previous studies in literature [5, 21].

From another perspective as shown Fig. 7, the hybrid FSO/RF transmission performs inefficiently regarding the energy issues. This phenomenon is understood by examining the functioning of the hybrid FSO/RF NTN. When the channel becomes unsuitable for the FSO link due to its failure to meet the necessary criteria as shown in Eq. (17e), HAP transitions to operating at RF frequency. Consequently, the power being transferred now exceeds the maximum power utilized for transmitting the signal via the FSO connection. According to formula (23), it is evident that an increase in transmitted power leads to a decrease in energy efficiency.

6. Conclusion

In this study, we proposed a JAMPC algorithm to improve the performance of FSO-based non-terrestrial networks. Particularly, we deeply focus on analyzing the energy efficiency of the proposed NTN over the combined channel taking into account the effects of atmospheric attenuation, cloud attenuation, geometric loss, and turbulence-induced fading. The numerical

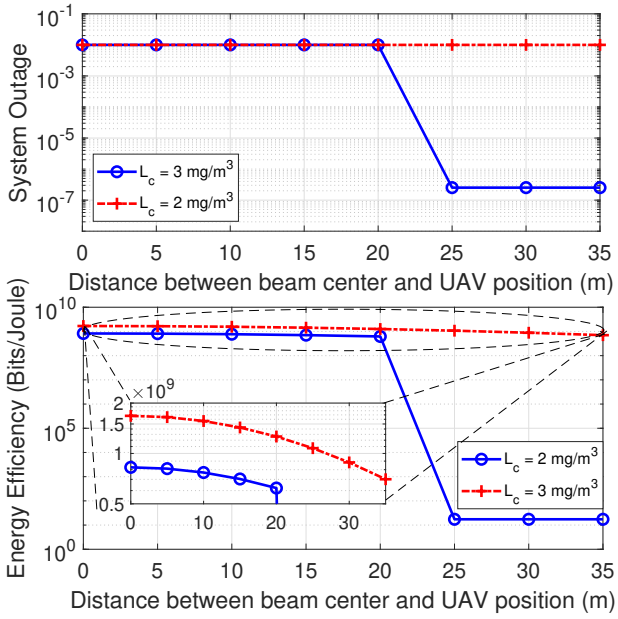

Figure 7. Investigation of implementing JAMPC for hybrid FSO/RF NTN under different cloud conditions.

results showed that the NTN using JAMPC has a larger energy efficiency than the conventional NTN with a fixed modulation size. The proposed JAMPC was also verified in various channel conditions to prove its feasibility.

Acknowledgement

This research was funded by the Vietnam Ministry of Information and Communications under Grant No. DT.09/24.

References

[1] ITU (Nov., 2023), Measuring digital development. facts and figures 2023, Tech. Rep. Int. Telecommun. Union (ITU), Geneva, Switzerland.

[2] Leyva-Mayorga, I., Soret, B., Röper, M., Wübben, D., Matthiesen, B., Dekorsy, A. and Popovski, P. (2020) Leo small-satellite constellations for 5g and beyond-5g communications. *IEEE Access* **8**: 184955–184964. doi:10.1109/ACCESS.2020.3029620.

[3] Samy, R., Yang, H.C., Rakia, T. and Alouini, M.S. (2022) Space-air-ground fso networks for high-throughput satellite communications. *IEEE Commun. Mag.* **60**(12): 82–87.

[4] Rahman, Z., Zafaruddin, S.M. and Chaubey, V.K. (2022) Multihop optical wireless communication over {-turbulence channels and generalized pointing errors with fog-induced fading. *IEEE Photonics J.* **14**(5): 1–14.

[5] Nguyen, T.V., Le, H.D., Dang, N.T. and Pham, A.T. (Nov. 2021) On the design of rate adaptation for relay-assisted

satellite hybrid FSO/RF systems. *IEEE Photonics J.* **14**(1): 1–11.

[6] Le, H.D. and Pham, A.T. (2022) On the design of fso-based satellite systems using incremental redundancy hybrid arq protocols with rate adaptation. *IEEE Trans. on Veh. Technol.* **71**(1): 463–477.

[7] Goldsmith, A. and Chua, S.G. (1997) Variable-rate variable-power mqam for fading channels. *IEEE Trans. on Commun.* **45**(10): 1218–1230.

[8] Lim, C.H. and Cioffi, J. (2001) Performance of the adaptive rate mqam with on/off power control. *IEEE Commun. Lett.* **5**(1): 16–18. doi:10.1109/4234.901812.

[9] Yu, W., Jia, H. and Musavian, L. (2022) Joint adaptive m-qam modulation and power adaptation for a downlink noma network. *IEEE Trans. on Commun.* **70**(2): 783–796.

[10] Karimi, M. and Uysal, M. (2012) Novel adaptive transmission algorithms for free-space optical links. *IEEE Trans. on Commun.* **60**(12): 3808–3815. doi:10.1109/TCOMM.2012.091012.110550.

[11] Le, H.D., Trinh, P.V., Pham, T.V., Kolev, D.R., Carrasco-Casado, A., Kubo-Oka, T., Toyoshima, M. *et al.* (Feb. 2022) Throughput analysis for TCP over the FSO-based satellite-assisted internet of vehicles. *IEEE Trans. Veh. Tech.* **71**(2): 1875–1890.

[12] Li, J., Yao, Y., Wu, G., Hou, J., Yu, W., Liu, B. and Liu, J. (Dec. 2019) Broadband laser doppler frequency shift emulator for satellite laser communication. *IEEE Photon. J.* **11**(6): 1–12.

[13] Yang, F., Cheng, J. and Tsiftsis, T.A. (Feb. 2014) Free-space optical communication with nonzero boresight pointing errors. *IEEE Trans. Commun.* **62**(2): 713–725.

[14] Nguyen, T.V., T. Le, H., Pham, H.T.T., Mai, V. and Dang, N.T. (2023) Enhancing design and performance analysis of satellite entanglement-based cv-qkd/fso systems. *IEEE Access* **11**: 112097–112107. doi:10.1109/ACCESS.2023.3323247.

[15] Fidler, F., Knapek, M., Horwath, J. and Leeb, W.R. (2010) Optical communications for high-altitude platforms. *IEEE J. Sel. Top. Quantum Electron.* **16**(5): 1058–1070. doi:10.1109/JSTQE.2010.2047382.

[16] Nguyen, T.V., Le, H.D., Dang, N.T. and Pham, A.T. (2021) Average transmission rate and outage performance of relay-assisted satellite hybrid fso/rf systems. In *2021 International Conference on Advanced Technologies for Communications (ATC)*: 1–6. doi:10.1109/ATC52653.2021.9598287.

[17] Le, H.D., Nguyen, T.V. and Pham, A.T. (2021) Cloud attenuation statistical model for satellite-based FSO communications. *IEEE Antennas Wirel. Propag. Lett.* **20**(5): 643–647. doi:10.1109/LAWP.2021.3058641.

[18] Erdogan, E. *et al.* (2021) Site diversity in downlink optical satellite networks through ground station selection. *IEEE Access* **9**: 31179–31190. doi:10.1109/ACCESS.2021.3059641.

[19] Gradshteyn, I.S. and Ryzhik, I.M. (2007) *Table of Integrals, Series, and Products, 7th Edition* (New York: Academic).

[20] Andrews, L.C. and Phillips, R.L. (2005) *Laser Beam Propagation through Random Media* (Bellingham, WA: SPIE Press), 2nd ed.

[21] Swaminathan, R., Sharma, S., Vishwakarma, N. and Madhukumar, A.S. (Jun. 2021) HAPS-based relaying for integrated space-air-ground networks with hybrid FSO/RF communication: A performance analysis. *IEEE Trans. Aerosp. Electron. Syst.* **57**(3): 1581–1599.

[22] ITU (2013), Attenuation due to clouds and fog, document Rec. ITU-R P-840-6.

[23] Simon, M. and Alouini, M. (2005) *Digital Communication over Fading Channels* (New York: John Wiley and Sons), 2nd ed.

[24] Rice, S.O. (1948) Statistical properties of a sine wave plus random noise. *The Bell Syst. Tech. J.* **27**(1): 109–157. doi:10.1002/j.1538-7305.1948.tb01334.x.

[25] Nguyen, T.V., Le, H.D. and Pham, A.T. (2023) On the design of ris–uav relay-assisted hybrid fso/rf satellite–aerial–ground integrated network. *IEEE Trans. Aerosp. Electron. Syst.* **59**(2): 757–771. doi:10.1109/TAES.2022.3189334.

[26] Singh, V., Solanki, S., Upadhyay, P.K., da Costa, D.B. and Moualeu, J.M. (2021) Performance analysis of hardware-impaired overlay cognitive satellite–terrestrial networks with adaptive relaying protocol. *IEEE Sys. J.* **15**(1): 192–203.

[27] Le, H.D., Mai, V.V., Nguyen, C.T. and Pham, A.T. (2018) Sliding window protocols with rate adaptation for fso burst transmission over turbulence channels. In *2018 International Conference on Information and Communication Technology Convergence (ICTC)*: 821–826. doi:10.1109/ICTC.2018.8539445.

[28] Boyd, S. and Vandenberghe, L. (2004) *Convex Optimization* (Cambridge, University Press).

[29] Kis, T. (2024) *Bisection Method* (Math Works, Available online at: https://www.mathworks.com).

[30] Adamchik, V. and Marichev, O. (1990) The algorithm for calculating integrals of hyperfeometric type functions and its realization in reduce system. In *Proc. Int. Conf. Symb. Algebraic Comput.*: 212–224.

[31] Abramowitz, M. and Stegun, I.A. (1972) *Handbook of Mathematical Functions, With Formulas, Graphs, and Mathematical Tables* (New York, USA: Dover), 9th ed.